J. Fluid Mech. (1987), *vol.* 175, *pp.* 511–535
Printed in Great Britain

The laminar boundary layer on a flat plate in periodic sideslip

By L. BERNSTEIN AND M. S. ISHAQ

Department of Aeronautical Engineering, Queen Mary College, University of London, Mile End Road, London E1 4NS, UK

(Received 21 February 1985 and in revised form 1 August 1986)

A theoretical study has been made of the laminar boundary layer on a semi-infinite flat plate parallel to a stream consisting of a uniform steady component U_∞ normal to its leading edge and a periodic sideslip component of the travelling-wave type, where the wave travels with velocity Q in the direction of the steady component. It is found that the longitudinal flow (that in planes perpendicular to the leading edge) is independent of the transverse flow, and satisfies the well-known Blasius equations. The transverse flow is governed by a linear partial differential equation which may be approximated in different ways for high and low values of the 'reduced' frequency $\bar{\omega}$. A series-expansion solution for small $\bar{\omega}$ appears to be valid up to about $\bar{\omega} = 2$; the solution for large $\bar{\omega}$ is applicable down to $\bar{\omega} \approx 10$. A third approximation has been developed which joins the others smoothly. Numerical solutions of the equations for the transverse flow are presented for $0 \leqslant \bar{\omega} \leqslant 40$ and $Q/U_\infty = 0.6$ (the value appropriate to the Queen Mary College (QMC) 'gust-tunnels') and for $\bar{\omega} = 10$ and $0.4 \leqslant Q/U_\infty \leqslant \infty$. The value of Q/U_∞ has a profound influence; for values less than about one there are large phase lags within the boundary layer; for large values there are phase leads throughout most of the layer. For $Q/U_\infty < 1$ the amplitude of the oscillation within the boundary layer exceeds that of the external driving oscillation, this 'overshoot' increasing as the wave-speed ratio diminishes. At $Q/U_\infty = 0.6$ peak velocities more than 3 times those outside appear within the viscous layer.

As $\bar{\omega} \to \infty$, the transverse viscous layer becomes thinner; the oscillatory boundary layer, here transverse, becomes a 'Stokes layer' and is virtually uncoupled from the longitudinal flow. Far downstream the amplitude of the transverse skin-friction grows as $x^{\frac{1}{2}}$ and becomes comparable with the streamwise component even for moderate values of the sideslip amplitude.

Experiments were conducted in one of the QMC gust-tunnels for values of $\bar{\omega}$ up to 2.0. Measurements of the transverse velocity amplitude and phase profiles confirm the 'low frequency theory'.

1. Introduction

The problem considered in this paper is that of a semi-infinite plate immersed in a stream of fluid having a uniform, steady component U_∞, normal to its leading edge and a periodic spanwise component w_∞, of the travelling-wave type, both in the plane of the plate. Travelling-wave flows are generated in the Queen Mary College (QMC) 'gust-tunnels' (see later) which have been developed specifically to study unsteady flows.

Periodic flows have been a subject of study since Stokes (1851) analysed the problem of an infinite plate oscillating harmonically in its own plane in an otherwise

stationary viscous fluid. There is now a large body of literature on unsteady viscous flows, and attention is drawn to the review by Stewartson (1960) and the recent book by Telionis (1981). Here we shall draw attention to a few of the main results relevant to periodic laminar boundary layers.

Lighthill (1954) investigated theoretically the response of a laminar boundary layer growing on a cylindrical body to sinusoidal fluctuations of the freestream velocity. Analysing the low- and high-frequency cases separately, he found that for small amplitudes, the velocity peak within the boundary layer was advanced in phase relative to the external stream by angles up to $\frac{1}{4}\pi$, the largest phase advance occurring at the plate (the wall). The phase advance increased with frequency, $\frac{1}{4}\pi$ being the asymptotic value for infinite frequency. Since the velocity at the wall is zero, the phase there is obtained from the velocity gradient, so, as Lighthill pointed out, the wall shear stress leads the external flow velocity maximum by up to $\frac{1}{4}\pi$. His main results were confirmed by Lin (1957) for high frequency and by Moore (1957) for low frequency, both of whom were able to remove the restriction to small amplitudes. At high frequencies the viscous effects are confined to a thin layer – the Stokes layer – adjacent to the wall; its thickness is of order $(\nu/\omega)^{\frac{1}{2}}$, where ν is the kinematic viscosity of the fluid and ω the radian frequency. Other studies have been reported by Nickerson (1957), Rott & Rosenzweig (1960), Ghosh (1961), Farn & Arpaci (1965), Teipel (1970), Ackerberg & Phillips (1972) and by Pedley (1972), the last of whom presented results for a plane wedge where the only restriction on the amplitude was that flow reversal should not occur. Experimental work by Hill & Stenning (1960) supports these studies.

A closely-related problem has been investigated by Patel (1975) and Lam (1983). The QMC gust-tunnels (Patel & Hancock 1976) are conventional low-speed wind-tunnels in which a periodic travelling-wave type of flow is generated by oscillating downstream extensions (flaps) attached to the roof and floor of the contraction nozzle. With the semi-open test-section relatively empty, in-phase harmonic oscillations of the flaps produce an upwash w, of the form

$$w = W_\infty(x,\omega)\sin\omega(t-x/Q), \tag{1}$$

where t is the time, Q is the travelling-wave velocity and the amplitude $W_\infty(x,\omega)$ varies both with drive frequency ω, and in some cases with distance x, along the tunnel. It is found experimentally that at sufficient distances downstream of the nozzle exit, $Q/U_\infty \approx 0.6$ for all frequencies (Ishaq 1984); here U_∞ is the mean longitudinal velocity component in the test-section.

With a splitter-plate parallel to the flaps in the flow, the periodicity takes the form of a longitudinal travelling-wave

$$U = U_\infty + \Delta U_\infty(x,\omega)\sin(t-x/Q). \tag{2}$$

In this configuration the vorticity shed from the flaps at the free edges of the jet has an image in the splitter-plate, thus creating a symmetrical flow pattern. Using this arrangement, Patel (1975, 1977) examined the behaviour of both laminar and turbulent boundary layers growing on a flat plate placed parallel to the flaps. He also extended Lighthill's (1954) analysis to the case of finite Q, and found broad agreement with his experimental results. The theory gives significantly different results depending upon whether Q is greater or less than U_∞. In particular the peak velocities reach much greater values for $Q < U_\infty$ and large phase lags occur within the boundary layer for $Q < U_\infty$ in contrast to the phase leads which occur for the standing-wave case. In fact Patel's (1975) analysis contained an error – he did not properly satisfy

the continuity equation – and Lam (1983) has obtained more accurate results. Using a differential-difference scheme, Lam (1983) obtained numerical solutions over a wide frequency range, and using $Q/U_\infty = 0.6$, he was able to improve considerably the agreement with Patel's experiments.

In the problem discussed here the flat plate is placed normal to the flaps in the gust tunnel, so that in addition to the steady component U_∞, in its own plane and perpendicular to its leading edge, there is the periodic spanwise component given by (1). The situation for which solutions are presented has $Q \to \infty$ as the special case already considered by Wuest (1952). We note that the longitudinal flow is independent of the transverse flow for all values of Q, a result found by Wuest (1952) for the standing-wave case and one which is well-known for the yawed semi-infinite plate in steady flow ($\omega = 0$), see Schlichting (1979).

The unsteady laminar boundary-layer equations with the given external flow are solved separately for small, intermediate and large values of the 'reduced' frequency $\bar{\omega} = \omega x/U_\infty$. At small values of $\bar{\omega}$, a regular expansion in powers of $\bar{\omega}$ reduces the partial differential equation for the transverse velocity to a set of ordinary differential equations that is solved numerically. The solution is found to be valid for $0 \leqslant \bar{\omega} \leqslant 2$ for all Q/U_∞. The high-frequency solution does not however 'match' at $\bar{\omega} = 2$, so a third approach is used in which the streamwise convection term is replaced by a finite difference representation, and the resulting ordinary differential equation is solved by 'marching downstream' from the already-computed solution at $\bar{\omega} = 1$, to match the high frequency solution at $\bar{\omega} = 10$. The details of the analysis are presented in §2, together with some results. They show features similar to those obtained by Patel (1975) and Lam (1983) for the longitudinal, travelling-wave type of flow. The value of Q/U_∞ has a marked effect, this time on the 'transverse boundary layer'. For low values of Q/U_∞ there are phase lags throughout most of the boundary layer, while for large values, the transverse velocity peak within the boundary layer leads that in the driving flow. For large values of $\bar{\omega}$, that is at high frequency or far downstream (if the boundary layer remains laminar), there is a 'Stokes layer', here transverse, accompanied by a boundary layer of conventional thickness. The results, which cover a wide range of values of Q/U_∞ and of $\bar{\omega}$, are discussed in §2. In practice only a limited number of values of Q/U_∞ are easily achieved, though the range of values of $\bar{\omega}$ is less restricted.

Some experiments conducted over the range $\bar{\omega} \leqslant 2$, are described in §3, where it is shown that they support the low-frequency analysis quite well.

2. The flat plate in oscillatory sideslip

2.1. *Analysis*

We consider a semi-infinite flat plate occupying the (x, z)-plane in the region $x \geqslant 0$, so that its leading edge lies along the axis Oz.

An incompressible fluid approaches the plate from $x = -\infty$ so that all velocity vectors lie in planes parallel to $y = 0$, and the velocity field there is given by

$$(u, v, w) = (U_\infty, 0, W_\infty \exp i\omega(t - x/Q)), \tag{3}$$

in which both W_∞ and Q are assumed constant. We investigate the flow in the region $x > 0$, $y \geqslant 0$, $-\infty < z < \infty$, see figure 1. Starting with the three-dimensional, unsteady laminar boundary-layer equations, and noting that for a plate of infinite span

$$\frac{\partial u}{\partial z} = \frac{\partial w}{\partial z} = 0,$$

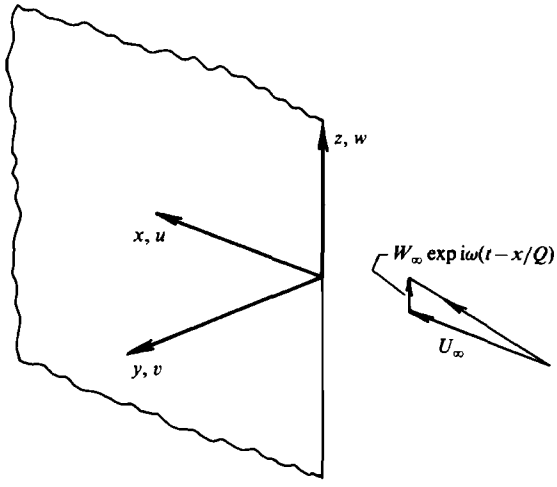

FIGURE 1. The semi-infinite flat plate in oscillatory sideslip.

but that
$$-\frac{1}{\rho}\frac{\partial p}{\partial z} = \frac{\partial w_\infty}{\partial t} + U_\infty \frac{\partial w_\infty}{\partial x} = \left(1-\frac{U_\infty}{Q}\right) i\omega w_\infty, \tag{4}$$

we obtain
$$\frac{\partial u}{\partial t} + u\frac{\partial u}{\partial x} + v\frac{\partial u}{\partial y} = \nu\frac{\partial^2 u}{\partial y^2}, \tag{5}$$

$$\frac{\partial w}{\partial t} + u\frac{\partial w}{\partial x} + v\frac{\partial w}{\partial y} = \left(1-\frac{U_\infty}{Q}\right) i\omega w_\infty + \nu\frac{\partial^2 w}{\partial y^2}, \tag{6}$$

$$\frac{\partial u}{\partial x} + \frac{\partial v}{\partial y} = 0, \tag{7}$$

subject to the boundary conditions

$$u = v = w = 0 \quad \text{at } y = 0, \tag{8}$$

and
$$u \sim U_\infty ; w \sim w_\infty = W_\infty \exp i\omega(t-x/Q) \quad \text{as } y \to \infty. \tag{9}$$

The solution of (5) and (7) subject to these boundary conditions gives $\partial u/\partial t = 0$ and the well-known Blasius solution. The longitudinal flow is thus independent of the transverse flow.

Since (6) is linear in w, we can write

$$w(x, y, t) = W_\infty g(x, y) \exp i\omega(t-x/Q), \tag{10}$$

so that
$$g(x, 0) = 0, \quad g(x, \infty) \to 1. \tag{11}$$

We now introduce the Blasius variables η and f, defined by

$$\eta = y\left(\frac{U_\infty}{2\nu x}\right)^{\frac{1}{2}} \quad \text{and } \psi(x, y) = (2x\nu U_\infty)^{\frac{1}{2}} f(\eta), \tag{12}$$

where ψ is the streamfunction satisfying (7), and obtain, after a little manipulation (see Bernstein 1984),

$$\frac{\partial^2 g}{\partial \eta^2} + f\frac{\partial g}{\partial \eta} + 2i\bar{\omega}\left(\frac{U_\infty}{Q} f' - 1\right) g = 2\bar{\omega} f' \frac{\partial g}{\partial \bar{\omega}} + 2i\bar{\omega}\left(\frac{U_\infty}{Q} - 1\right), \tag{13}$$

with the boundary conditions

$$g(\bar{\omega}, 0) = 0 \quad \text{and } g(\bar{\omega}, \infty) \to 1. \tag{14}$$

The function $f(\eta)$ is known (numerically) from the solution of the Blasius equation $f''' + ff'' = 0$ with $f(0) = f'(0) = 0$ and $f'(\infty) \to 1$. The dash denotes differentiation with respect to η.

Equations (13) and (14) have no general analytic solution, but we may examine the asymptotic cases of high and low frequency. We note that applying the wall boundary conditions to (13) leads to

$$\left[\frac{\partial^2 g}{\partial \eta^2}\right]_{\eta=0} = 2\mathrm{i}\bar{\omega}\left(\frac{U_\infty}{Q} - 1\right),$$

so we may expect some critical dependence on Q/U_∞.

2.2. *High-frequency solution*

2.2.1. *Outer region*

If we take the simple limit of (13) as $\bar{\omega} \to \infty$, the differential terms vanish and we obtain as a first approximation in the outer region of the boundary layer

$$g = \frac{U_\infty - Q}{U_\infty f' - Q} = \frac{U_\infty - Q}{u - Q}. \tag{15}$$

Since $u(\eta)$ has the Blasius profile, there is a singularity within the boundary layer if $Q < U_\infty$. One is tempted to seek a series solution in inverse powers of $\bar{\omega}$ in the outer region. Writing

$$g(\bar{\omega}, \eta) = \sum_{r=0}^{\infty} \bar{G}_r(\eta)\, \bar{\omega}^{-r},$$

we find $G_0(\eta)$ is given by (15) and $G_1(\eta)$ by

$$G_1 = -\mathrm{i} f''^2 \left(1 - \frac{Q}{U_\infty}\right) \frac{Q}{U_\infty} \left(f' - \frac{Q}{U_\infty}\right)^{-4},$$

with succeeding terms having even higher-order singularities at $u = Q$. There is thus a critical layer around $\eta = \eta_c$, where η_c is defined by $u(\eta_c) = Q$. We shall return to this point shortly.

2.2.2. *Near-wall region*

The outer solution does not satisfy the wall boundary condition of no slip. Near the wall $f' \approx f \approx 0$ to first order and (13) may be approximated by

$$\frac{\mathrm{d}^2 g}{\mathrm{d}\eta^2} - 2\mathrm{i}\bar{\omega} g \approx 2\mathrm{i}\bar{\omega}\left(\frac{U_\infty}{Q} - 1\right). \tag{16}$$

The solution which satisfies $g(\bar{\omega}, 0) = 0$ is

$$g = \left(1 - \frac{U_\infty}{Q}\right)\{1 - \exp[-(1+\mathrm{i})\bar{\omega}^{\frac{1}{2}}\eta]\}, \tag{17}$$

where the exponentially-growing term has been neglected. This is of the same form as Lighthill's (1954) solution for the velocity fluctuations in a laminar boundary layer subject to an oscillation of the form $U(x,t) = U_\infty + \Delta U_\infty \exp \mathrm{i}\omega t$, the only difference being the presence here of the term U_∞/Q. But for the scaling factor $(1 - U_\infty/Q)$, which is negative for $Q < U_\infty$, the transverse velocity profiles here are similar to the

streamwise profiles obtained by Lighthill (1954) and Lin (1957). It is interesting that while Lighthill's high-frequency solution satisfies both boundary conditions, (17) satisfies the condition at the wall, but not $g(\infty)\to 1$; in fact (16) cannot accommodate such an outer condition (unless $Q=\infty$), and could only be valid near the wall.†

An improved approximation near the wall may be obtained‡ by noting that at high frequency the Stokes lengthscale $(\nu/\omega)^{\frac{1}{2}}$ is much smaller than the Blasius lengthscale $(2\nu x/U_\infty)^{\frac{1}{2}}$, so that a new variable

$$\zeta = y\left(\frac{\omega}{2\nu}\right)^{\frac{1}{2}} = \eta\bar{\omega}^{\frac{1}{2}},$$

may be introduced.

Close to the wall we may use the approximation

$$f(\eta) = \tfrac{1}{2}f''(0)\,\eta^2 + O(\eta^5),$$

where $f''(0) = 0.4696$.

Equation (13), written in terms of ζ then becomes

$$\frac{\mathrm{d}^2 g}{\mathrm{d}\zeta^2} + \tfrac{1}{2}\bar{\omega}^{-\frac{3}{2}}f''(0)\,\zeta^2\frac{\mathrm{d}g}{\mathrm{d}\zeta} + 2\mathrm{i}\left(\frac{U_\infty}{Q}\zeta f''(0)\,\bar{\omega}^{-\frac{1}{2}} - 1\right)g$$
$$= \left\{2\bar{\omega}^{-\frac{3}{2}}f''(0)\,\zeta\left(\bar{\omega}\frac{\mathrm{d}g}{\mathrm{d}\bar{\omega}} + \tfrac{1}{2}\zeta\frac{\mathrm{d}g}{\mathrm{d}\zeta}\right)\right\} + 2\mathrm{i}\left(\frac{U_\infty}{Q} - 1\right), \quad (18)$$

The form of this equation suggests the expansion

$$g(\bar{\omega},\zeta) = \sum_{r=0}^{\infty} G_r(\zeta)\,\bar{\omega}^{-\frac{1}{2}r}, \quad (19a)$$

with $$g(\bar{\omega},0) = 0, \quad g(\bar{\omega},\infty)\to 1 - \frac{U_\infty}{Q}.$$

Substituting into (18) and equating like powers of $\bar{\omega}^{-\frac{1}{2}}$ yields

$$\left.\begin{aligned} G_0(\zeta) &= \left(1-\frac{U_\infty}{Q}\right)\{1-\mathrm{e}^{-(1+\mathrm{i})\zeta}\},\\ G_1(\zeta) &= f''(0)\frac{U_\infty}{Q}\left(1-\frac{U_\infty}{Q}\right)\zeta[1-\tfrac{1}{4}\{1+(1+\mathrm{i})\,\zeta\}\,\mathrm{e}^{-(1+\mathrm{i})\zeta}],\end{aligned}\right\} \quad (19b)$$

etc.

G_0 is the first approximation given by (17). For large ζ (corresponding to large $\bar{\omega}$ but small η) substitution into (19a) gives

$$g(\bar{\omega},\eta) = \left(1-\frac{U_\infty}{Q}\right)\left[1+\eta f''(0)\frac{U_\infty}{Q}+\ldots\right] \quad \text{for } \eta>0, \quad (19c)$$

which matches to this order in η, the behaviour near the wall of the outer solution, (15), when u/U_∞ is written as $\eta f''(0)$.

The transverse shear stress at the wall is proportional to $(\mathrm{d}g/\mathrm{d}\eta)_{\eta=0} = g'(0)$, so that

$$g'(0) = \bar{\omega}^{\frac{1}{2}}\left(\frac{\mathrm{d}g}{\mathrm{d}\zeta}\right)_{\zeta=0} = \bar{\omega}^{\frac{1}{2}}\left(1-\frac{U_\infty}{Q}\right)\left\{(1+\mathrm{i}) + \tfrac{3}{4}\bar{\omega}^{-\frac{1}{2}}f''(0)\frac{U_\infty}{Q} + O(\bar{\omega}^{-\frac{3}{2}})\right\}. \quad (20)$$

† Rott & Rosenzweig (1960) discuss an analogous problem in relation to higher-order expansions for Lighthill's problem.

‡ We are indebted to T. J. Pedley for pointing this out and also for the discussion on the critical layer which follows.

The relative phase $\phi_w = \phi(0) - \phi(\infty)$ at the wall is given, using L'Hôpital's rule, by

$$\tan\phi_w = \frac{\operatorname{Im} g'(0)}{\operatorname{Re} g'(0)} = \left\{1 + \frac{3}{4}\frac{U_\infty}{Q} f''(0)\,\bar{\omega}^{-\frac{1}{2}} + \ldots\right\}^{-1} \tag{21}$$

so that for $\bar{\omega} \to \infty$

$$\phi_w = \tfrac{1}{4}\pi \quad \text{for } Q/U_\infty > 1,$$

$$\phi_w = -\tfrac{3}{4}\pi \quad \text{for } Q/U_\infty < 1.$$

Equation (21) suggests a variation of only a few degrees over the range $10 \leqslant \bar{\omega} \leqslant \infty$, rather smaller than that given by the numerical solution at high frequency (see later) from which it departs for $\bar{\omega} < 40$ at $Q/U_\infty = 0.6$.

2.2.3. *Critical layer*

For $Q < U_\infty$ the inviscid solution breaks down near $\eta = \eta_c$. In this region, where $u \approx Q$, we may write

$$f'(\eta) - Q/U_\infty = (\eta - \eta_c) f''(\eta_c) + O(\eta - \eta_c)^2,$$

and the viscous term in (13) will be of the same order of magnitude as the other terms. Rescaling as follows:

$$\bar{\eta} = \bar{\omega}^{\frac{1}{3}}(\eta - \eta_c), \quad \bar{g} = \bar{\omega}^{-\frac{1}{3}} g,$$

and noting that the $\bar{\omega}(\mathrm{d}g/\mathrm{d}\bar{\omega})$ term in (13) is of order $\bar{\omega}^{-\frac{2}{3}}$ times the leading term, we write

$$\bar{g}(\bar{\omega}, \bar{\eta}) = \bar{g}_0(\bar{\eta}) + \bar{\omega}^{-\frac{1}{3}} \bar{g}_1(\bar{\eta}) + \ldots$$

and calculate only the leading term $\bar{g}_0$, for large $\bar{\omega}$.

The equation for $\bar{g}_0$ is then

$$\frac{\mathrm{d}^2 \bar{g}_0}{\mathrm{d}\bar{\eta}^2} + 2\mathrm{i}\alpha \frac{U_\infty}{Q} \bar{\eta} \bar{g}_0 = 2\mathrm{i}\left(\frac{U_\infty}{Q} - 1\right) \tag{22}$$

where $\alpha = f''(\eta_c)$.

Equation (22) is essentially Airy's equation. Writing

$$\xi = \left(\frac{2\alpha U_\infty}{Q}\right)^{\frac{1}{3}} \bar{\eta}\mathrm{i}, \quad \tilde{g}_0 = \frac{\mathrm{i}}{2\pi}\left(\frac{2\alpha U_\infty}{Q}\right)^{\frac{2}{3}} \left(\frac{U_\infty}{Q} - 1\right)^{-1} \bar{g}_0,$$

it becomes

$$\frac{\mathrm{d}^2 \tilde{g}_0}{\mathrm{d}\xi^2} - \xi \tilde{g}_0 = \pi^{-1},$$

the appropriate solution of which is given by Abramowitz & Stegun (1965) as

$$\tilde{g}_0 = \mathrm{Hi}(\xi) = \frac{1}{\pi} \int_0^\infty \exp\{-\tfrac{1}{3}t^3 + \xi t\}\,\mathrm{d}t \tag{23}$$

which has the required property that

$$\bar{g}_0 \sim \frac{\left(1 - \dfrac{Q}{U_\infty}\right)}{\alpha \bar{\eta}} \quad \text{as } \xi \to \pm\mathrm{i}\infty.$$

One may note that $\pi \mathrm{Hi}(0) \approx 1.28790$, so that

$$g_0(\eta_c) \approx 2.5758\mathrm{i}\left(1 - \frac{U_\infty}{Q}\right)\left(\frac{2\alpha U_\infty}{Q}\right)^{-\frac{2}{3}} \bar{\omega}^{\frac{1}{3}}. \tag{24}$$

Thus for $Q < U_\infty$, the relative phase $\phi(\eta_c) - \phi(\infty) \to -\frac{1}{2}\pi$ for large values of $\bar{\omega}$.

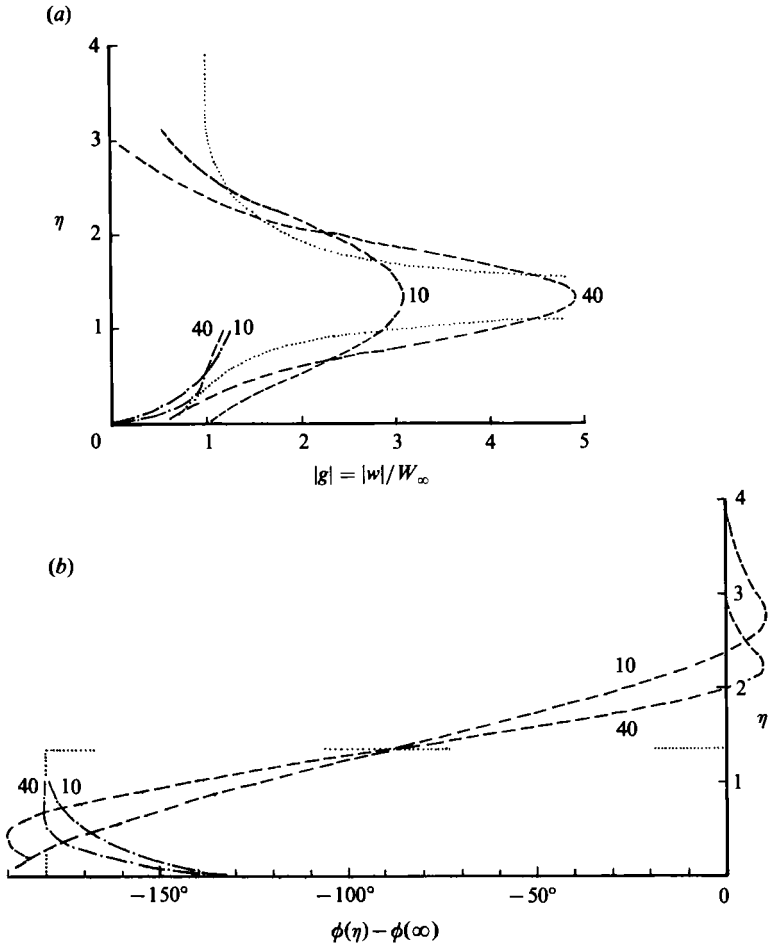

FIGURE 2. Sideslip velocity (*a*) amplitude profiles, (*b*) relative phase profiles, for $Q/U_\infty = 0.6$. ·····, outer solution, equation (15); —·—·—, near-wall solution, equations (19); – – – –, critical layer solution, equation (23). Numbers on curves indicate values of $\bar{\omega}$.

The velocity profiles given by (15), (19) and (23) are shown, for $Q/U_\infty = 0.6$ and $\bar{\omega} = 10$ and 40, in figure 2.

It can be seen that the critical layer analysis successfully smooths out the discontinuity of (15) in the neighbourhood of η_c, but it does not possess the correct behaviour either near the wall, $\eta = 0$, or far from it, $\eta \to \infty$. Nor does the solution join the near-wall solution smoothly for the two values of $\bar{\omega}$ computed, although one may note that even at $\bar{\omega} = 40$, the near-wall solution is almost tangent to the outer inviscid solution, equation (15), as is suggested by (19*c*) for $\bar{\omega} \to \infty$.

2.2.4. *Numerical solution*

A single solution, valid throughout the boundary layer may be obtained numerically with relative ease after first reducing (13) to an ordinary differential equation. In the near-wall region, the term that arises from the convective derivative $\mathrm{d}g/\mathrm{d}\bar{\omega}$, that is, the term in { } on the right-hand side of (18), is small. In the critical layer region it is $\bar{\omega}^{-\frac{2}{3}}$ times the leading term in the equation, and it is clearly small in the

outer region. Thus for $\bar{\omega}$ large, we neglect the convective term, (13) becomes an ordinary differential equation, and if we write

$$g(\eta) = g_{\mathrm{R}}(\eta) + ig_{\mathrm{i}}(\eta), \tag{25}$$

and substitute into (13) and (14), we obtain the coupled equations

$$g_{\mathrm{R}}'' + fg_{\mathrm{R}}' + 2\bar{\omega}g_{\mathrm{i}}\left(1 - \frac{U_\infty}{Q}f'\right) = 0, \tag{26a}$$

and

$$g_{\mathrm{i}}'' + fg_{\mathrm{i}}' - 2\bar{\omega}g_{\mathrm{R}}\left(1 - \frac{U_\infty}{Q}f'\right) = 2\bar{\omega}\left(1 - \frac{U_\infty}{Q}\right), \tag{26b}$$

for the real and imaginary parts, with

$$\left.\begin{aligned} g_{\mathrm{i}}(0) = g_{\mathrm{i}}(\infty) = g_{\mathrm{R}}(0) = 0, \\ g_{\mathrm{R}}(\infty) = 1. \end{aligned}\right\} \tag{27}$$

Equations (26) and (27) together with the Blasius equation for f have been solved numerically, using a fourth-order, Runge–Kutta technique on a microcomputer (Hewlett–Packard, HP 9826A), for $Q/U_\infty = 0.6$ and a range of values of $\bar{\omega}$. Solutions were also obtained for several other values of Q/U_∞ in the range of 0.4 to ∞, at $\bar{\omega} = 10$. In all computations the outer boundary conditions were applied at $\eta = 10$. Computational accuracy diminishes as $\bar{\omega}$ increases for reasons explained by Bernstein (1984). Some of the results for $Q = 0.6U_\infty$, are shown in figure 3, the normalized sideslip amplitude profiles $|g| = |w|/W_\infty$ being shown in figure 3 (*a*) and the relative phase $[\phi(\eta) - \phi(\infty)]$ in figure 3 (*c*). Also shown for comparison in figure 3 are the critical layer solution, equations (23) and (24) for $\bar{\omega} = 10$ and 40.

The velocity profiles exhibit a very marked 'overshoot' in the magnitude, which increases with $\bar{\omega}$. The peak value occurs in the region near which $Q = u$, as is suggested by the outer solution; the peak values $\hat{g}(\bar{\omega})$, shown in figure 3 (*b*), are well predicted by the critical layer analysis, which is also accurate over much of the 'inner region', even for $\bar{\omega}$ as small as 10.

The relative phase shows a wide variation through the boundary layer, the response lagging the excitation through most of it. There are however, small phase leads, $\phi(\eta) > \phi(\infty)$, in the outer region for all values of $\bar{\omega}$, and in a thin inner region, but not adjacent to the wall, for the larger values of $\bar{\omega}$ there are phase leads approaching 180° (lags exceeding 180°). For $\bar{\omega} \geqslant 10$, the phase profiles have a common crossing point at $\eta \approx 1.337$ (for $Q/U_\infty = 0.6$) the point where $Q = u$. The phase lag is however slightly less than the 90° predicted by the critical layer approximation.

Computations at $Q/U_\infty = 0.9$ do not exhibit a similar characteristic at these values of $\bar{\omega}$, while for $Q/U_\infty < 0.6$, the phase lag is close to 90° at $\eta = \eta_{\mathrm{c}}$, presumably due to the importance of the factor $(1 - U_\infty/Q)$.

Figure 4 shows solutions for several values of Q/U_∞ and for $\bar{\omega} = 10$. The profiles change markedly with Q/U_∞, further data, not shown for clarity, showing that $Q = U_\infty$ is *not* the critical value (see Bernstein 1984). As Q/U_∞ becomes large the region of appreciable sideslip-velocity-gradient amplitude becomes thinner, see figure 4 (*a*); although not shown for clarity, it also narrows with increasing $\bar{\omega}$. Since $\bar{\omega}$ $(= \omega x/U_\infty)$ may be regarded as either a frequency parameter or a streamwise coordinate, the transverse shear stress $\mu(\partial w/\partial y)$ response is only significant in a

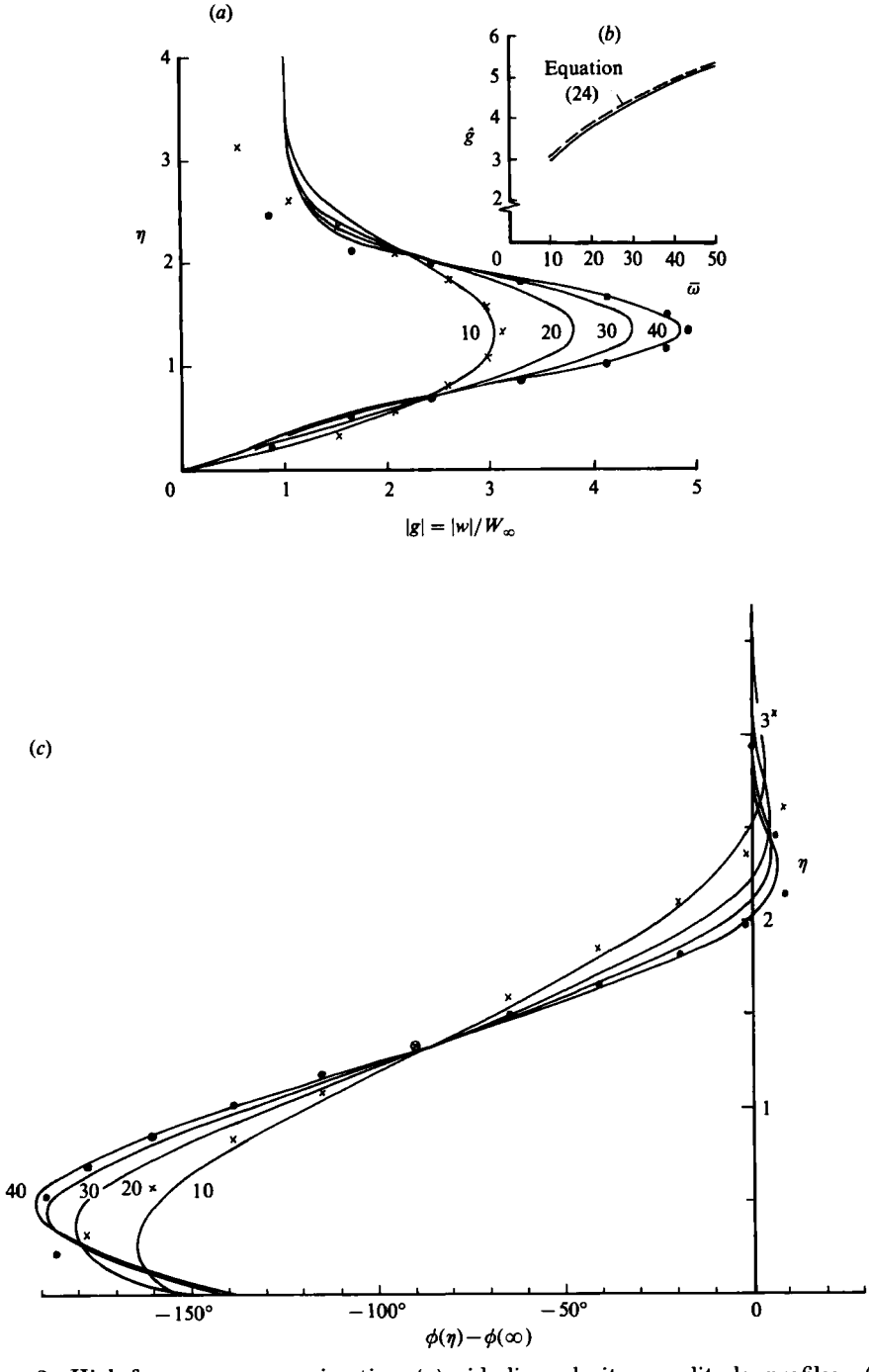

FIGURE 3. High-frequency approximation (*a*) sideslip velocity amplitude profiles; (*b*) peak velocities; (*c*) relative phase profiles. Numbers on curves indicate values of $\bar{\omega}$. ●, critical layer solution $\bar{\omega} = 40$; ×, critical layer solution $\bar{\omega} = 10$.

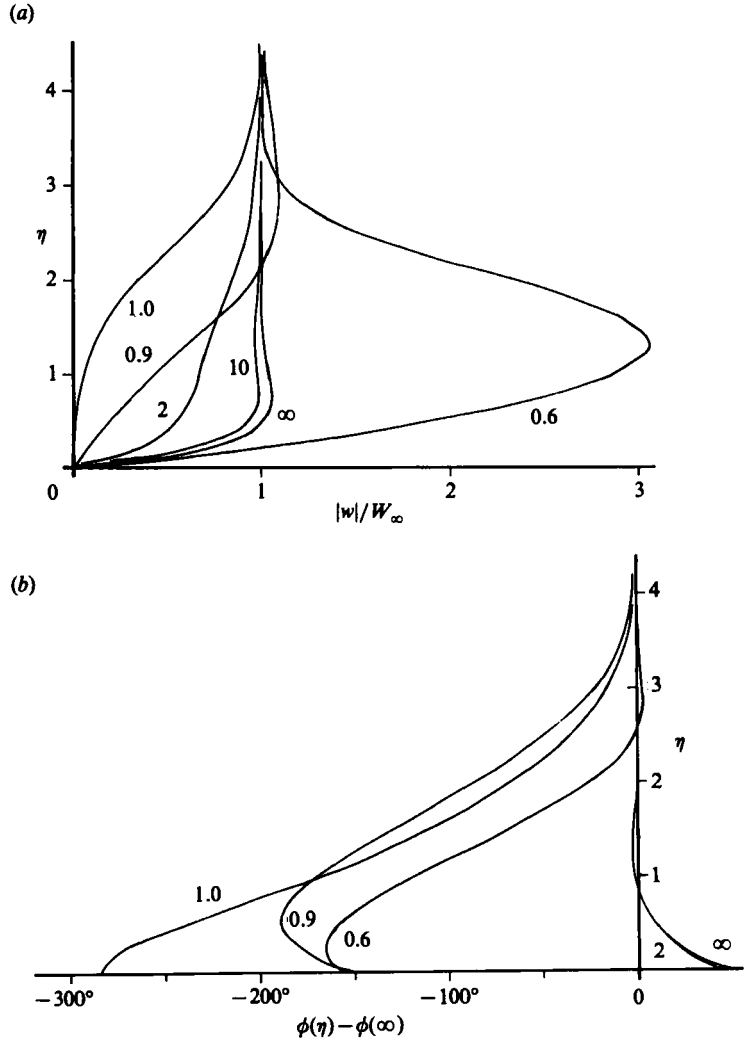

FIGURE 4. (*a*) Normalized sideslip amplitude profiles and, (*b*) relative phase angle profiles for $\bar{\omega} = 10$ and the values of Q/U_∞ indicated.

narrow region close to the wall for either large x or large ω (or both). This is analogous to the 'Stokes shear layer' which appears for streamwise oscillations of a plate in its own plane in company with a rather thicker, conventional steady boundary layer growing in the mainstream $0x$-direction; here however, the Stokes layer is transverse. Before leaving this high-frequency solution, we note that the assumption that $\bar{\omega}(\partial g/\partial\bar{\omega})$ becomes negligible as $\bar{\omega}$ becomes large, is justified by the results; $g''(\eta)$ is at least an order of magnitude larger than $\bar{\omega}f'(\Delta g/\Delta\bar{\omega})$ for $\bar{\omega} \geqslant 10$. We shall return to this point in §2.4.

2.3. *Low-frequency solution*

For small values of the frequency parameter $\bar{\omega}$ we assume that $g(\bar{\omega}, \eta)$ may be expanded as a power series in $(\mathrm{i}\bar{\omega})$. Thus

$$g(\bar{\omega}, \eta) = \sum_{r=0} (\mathrm{i}\omega)^r g_r(\eta). \tag{28}$$

Substituting into (13), and again using a prime to denote differentiation with respect to η, leads to the following set of equations, in addition to the Blasius equation:

$$g_0 + f g_0' = 0, \tag{29}$$

$$g_1'' + f g_1' - 2 f' g_1 = 2\left(1 - \frac{U_\infty}{Q} f'\right) g_0 + 2\left(\frac{U_\infty}{Q} - 1\right), \tag{30}$$

$$g_r'' + f g_r' - 2 r f' g_r = 2\left(1 - \frac{U_\infty}{Q} f'\right) g_{r-1} \quad \text{for } r > 1, \tag{31}$$

and the boundary conditions are

$$\left.\begin{aligned} &g_r(0) = 0 \quad \text{for all } r, \\ &g_0(\infty) \to 1, \\ &g_r(\infty) \to 0 \quad \text{for } r > 0. \end{aligned}\right\} \tag{32}$$

The solution of (29) subject to these boundary conditions is clearly

$$g_0(\eta) = f'(\eta), \tag{33}$$

so that the steady-state solution ($\omega = 0$) satisfies the Blasius equation as may be expected (see Schlichting 1979).

With $g_0(\eta)$ known, (30) for $g_1(\eta)$ may be solved, followed sequentially by g_2, g_3, etc.

Equations (29) to (32) have been solved up to $r = 8$ on the HP 9826A using a fourth-order Runge–Kutta, a common algorithm being used for all but the first equation. Solutions have been obtained for several values of Q/U_∞ including 0.6 and infinity. Again the outer boundary conditions were applied at $\eta = 10$. By separating the real and imaginary parts of equation (28) for $g(\bar{\omega}, \eta)$, the phase $\phi(\bar{\omega}, \eta)$ relative to the local external flow can be obtained as

$$\phi(\bar{\omega}, \eta) - \phi(\bar{\omega}, \infty) = \tan^{-1}\left\{\frac{\bar{\omega} g_1 - \bar{\omega}^3 g_3 + \bar{\omega}^5 g_5 - \dots}{g_0 - \bar{\omega}^2 g_2 + \bar{\omega}^4 g_4 - \dots}\right\}. \tag{34}$$

Since however $g_r(0) = 0$ for all r, the relative phase ϕ_w, at the wall is obtained using

$$\phi_w = \phi(\bar{\omega}, 0) - \phi(\bar{\omega}, \infty) = \tan^{-1}\left\{\frac{\sum_{r=1} (-1)^{r-1} \bar{\omega}^{(2r-1)} g_{2r-1}'(0)}{\sum_{r=1} (-1)^{r-1} \bar{\omega}^{2(r-1)} g_{2(r-1)}'(0)}\right\}. \tag{35}$$

Because the integration of (31) for g_r depends upon the solution for g_{r-1}, accuracy gradually decreases due to rounding errors. Such errors will limit the range of $\bar{\omega}$ over which this low-frequency solution may be applied, although in so far as the functions $g_r(\eta)$ are in general nearly an order of magnitude smaller than $g_{r-1}(\eta)$ for $r > 5$, see Bernstein (1984), one would expect the results to be inherently applicable well above $\bar{\omega} = 1$. At the lower end we have noted that $\bar{\omega} = 0$ gives the known steady-state solution. Here we must interpret $\bar{\omega} = 0$ as appropriate to $\omega = 0$ and not $x = 0$, since the boundary-layer equations do not apply close to the leading edge of the plate.

Figure 5(*a*) illustrates the sideslip velocity amplitude profiles and figure 5(*b*) the relative phase profiles for $Q/U_\infty = 0.6$ and for $0 \leqslant \bar{\omega} \leqslant 2$. The rounding errors referred to earlier begin to be significant for $\bar{\omega} > 2$. Similar results have been obtained for other values of the wave-speed ratio, some of those for $Q/U_\infty \to \infty$ being shown in figure 6. It will be noticed that whereas the velocity amplitude profiles are

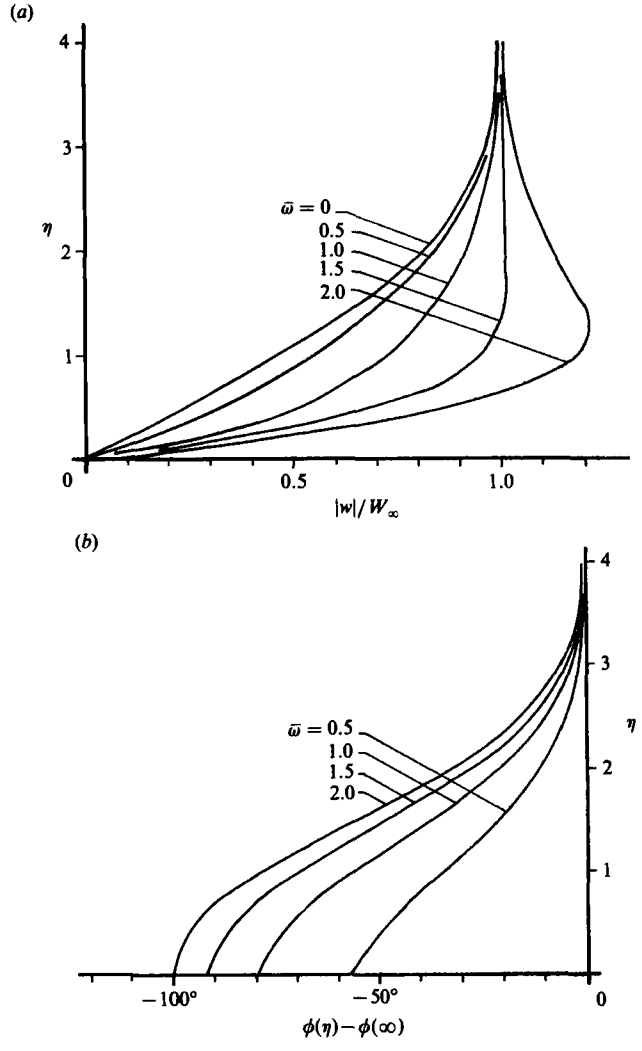

FIGURE 5. Sideslip velocity profiles for $Q/U_\infty = 0.6$; low-frequency solution: (*a*) normalized amplitude, (*b*) relative phase angle.

relatively insensitive to the wave-speed ratio, the relative phase changes from a lag for $Q/U_\infty = 0.6$ to a phase lead for $Q/U_\infty \to \infty$. The results for $Q/U_\infty = 1$, not reproduced, show that the amplitude profiles for $0 \leqslant \bar{\omega} \leqslant 2$ are insensitive to $\bar{\omega}$, but there are velocity lags within the boundary layer relative to the driving oscillation. At $Q/U_\infty = 2$, also not shown, the velocity inside the boundary layer leads that outside. The change from phase lead to lag at the wall, appears to occur at $Q/U_\infty \approx 1.23$ for $0 \leqslant \bar{\omega} < 1$, though this is weakly dependent upon $\bar{\omega}$. Even though $\phi_w \approx 0$, there are small phase lags away from the surface at this wave-speed ratio.

2.4. *Intermediate frequency solution*

In §2.2 results were presented for the high-frequency approximation for $\bar{\omega} \geqslant 10$, while in §2.3 we have seen that the low-frequency approximation gives results for the range $0 < \bar{\omega} < 2$; in fact for $Q/U_\infty = 0.6$, the latter solution seems to be not too seriously

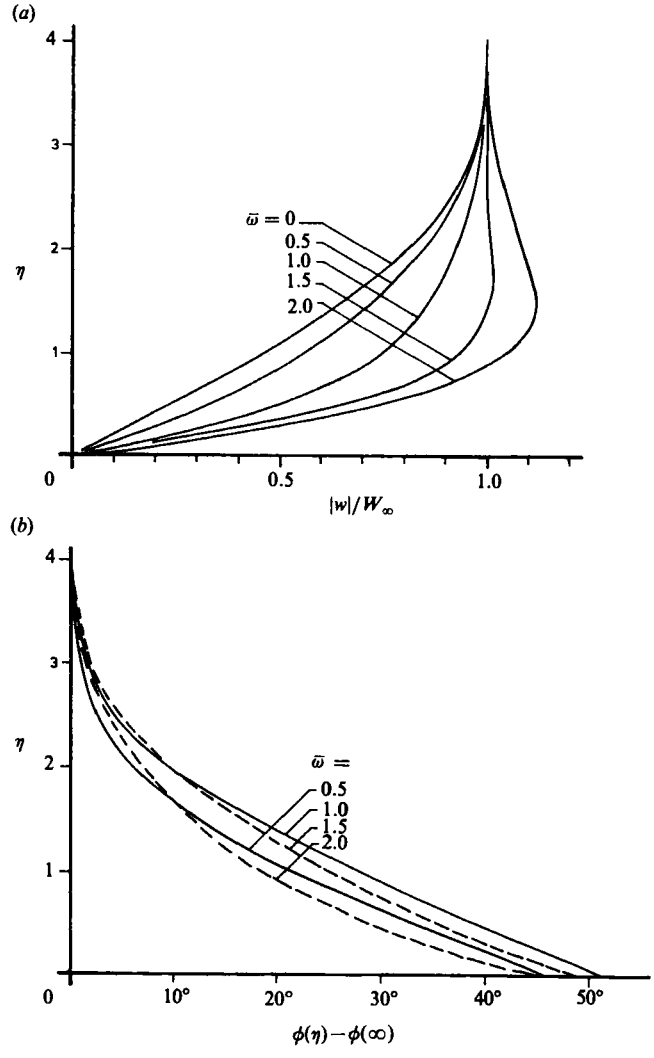

FIGURE 6. Sideslip velocity profiles for $Q/U_\infty = \infty$; low-frequency solution.

affected by rounding errors up to about $\bar{\omega} = 3$. The questions that arise however are: what is the lower limit of $\bar{\omega}$ for which the high frequency approximation may be used? and what happens in the intermediate frequency parameter range?

Computations have been carried out using the high frequency approximation for values of $\bar{\omega}$ down to 1. Figure 7 shows comparisons, for $Q/U_\infty = 0.6$, of the high- and low-frequency approximations to the velocity amplitude profiles at $\bar{\omega} = 1$, 2 and 3. It is clear that they differ widely from one another, as there is no overlap region. Figure 8 shows the relative phase ϕ_w, at the wall, throughout the range of $\bar{\omega}$ for $Q/U_\infty = 0.6$. The discrepancy in the range $1 < \bar{\omega} < 3$ between the two solutions is not large, but the solutions show no sign of joining smoothly.

Both the high- and low-frequency approximations depend upon assumptions which reduce the partial differential equation (13) to sets of ordinary differential equations. This considerably eases the problem of numerical solution; indeed it makes solution possible on a microcomputer. The direct solution of (13) using a finite difference

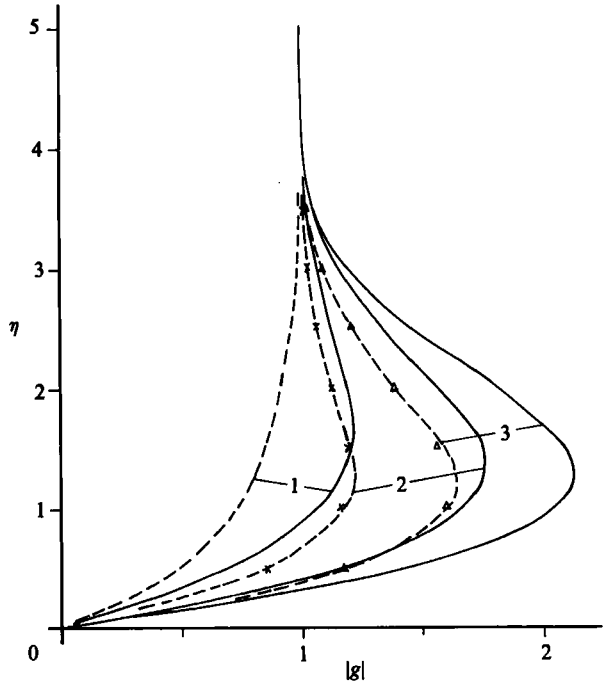

FIGURE 7. Normalized sideslip amplitude profiles for values of $\bar{\omega}$ indicated: ——, high-frequency solution; – – – –, low-frequency solution; (symbols are intermediate frequency solution) ×, $\bar{\omega} = 2$; △, $\bar{\omega} = 3$.

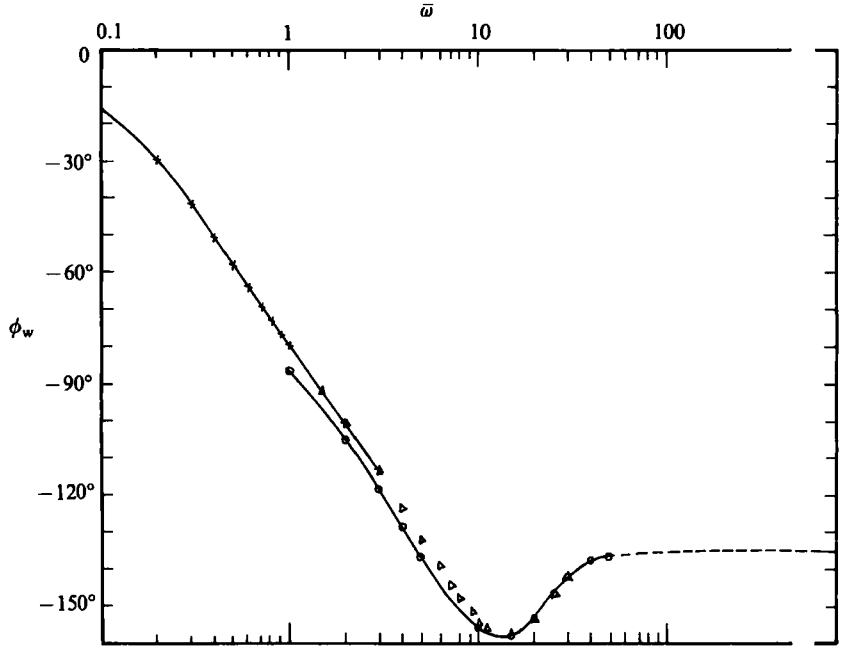

FIGURE 8. Relative phase angle ϕ_w at the wall for $Q/U_\infty = 0.6$; — × — × —, low-frequency solution; —○—○—, high-frequency solution; ▷, intermediate-frequency solution. The asymptotic value is given by equation (21).

representation is less practical on such a machine. A hybrid approach is however possible, as follows.

The streamwise convection term $2\bar{\omega}f'(\partial g/\partial\bar{\omega})$ in (13) is expressed in finite difference form as

$$2\bar{\omega}f'\frac{\Delta g(\bar{\omega},\eta)}{\Delta\bar{\omega}} = 2\bar{\omega}f'\frac{[g(\bar{\omega}+\Delta\bar{\omega},\eta)-g(\bar{\omega},\eta)]}{\Delta\bar{\omega}}. \tag{36}$$

We now suppose that $g(\bar{\omega},\eta)$ is known and $g(\bar{\omega}+\Delta\bar{\omega},\eta)$ is to be found, and since g satisfies (13), we write the latter, using (36) as

$$g''+fg'+2\mathrm{i}\bar{\omega}\left(\frac{U_\infty}{Q}f'-1\right)g-\frac{2\bar{\omega}}{\Delta\bar{\omega}}f'g = 2\mathrm{i}\bar{\omega}\left(\frac{U_\infty}{Q}-1\right)-\frac{2\omega}{\Delta\bar{\omega}}f'g(\bar{\omega},\eta), \tag{37}$$

where $g = g(\bar{\omega}+\Delta\bar{\omega},\eta)$ and dashes denote differentiation with respect to η. If an initial value of $\bar{\omega}$ is chosen at which the solution $g(\bar{\omega},\eta)$ is known, the solution at $(\bar{\omega}+\Delta\bar{\omega})$ may be computed using a standard Runge–Kutta procedure to integrate (37). Because $\bar{\omega}$ represents the streamwise coordinate, this is equivalent to computing the flow at $(x+\Delta x)$ from the known flow at the upstream station x.

Again we separate the real and imaginary parts of g, writing

$$g(\bar{\omega}+\Delta\bar{\omega},\eta) = G(\bar{\omega}+\Delta\bar{\omega},\eta)+\mathrm{i}H(\bar{\omega}+\Delta\bar{\omega},\eta), \tag{38}$$

and (37) becomes the coupled pair

$$G_n''+fG_n'-\frac{2\bar{\omega}}{\Delta\bar{\omega}}f'G_n-2\bar{\omega}\left(\frac{U_\infty}{Q}f'-1\right)H_n = -\frac{2\bar{\omega}}{\Delta\bar{\omega}}f'G_{n-1}, \tag{39}$$

and

$$H_n''+fH_n'-\frac{2\bar{\omega}}{\Delta\bar{\omega}}f'H_n+2\bar{\omega}\left(\frac{U_\infty}{Q}f'-1\right)G_n = 2\bar{\omega}\left(\frac{U_\infty}{Q}-1-\frac{f'H_{n-1}}{\Delta\bar{\omega}}\right), \tag{40}$$

with the boundary conditions

$$\left.\begin{aligned} &G(\bar{\omega}+\Delta\bar{\omega},0) = H(\bar{\omega}+\Delta\bar{\omega},0) = H(\bar{\omega}+\Delta\bar{\omega},\infty) = 0,\\ \text{and}\quad &G(\bar{\omega}+\Delta\bar{\omega},\infty)\to 1. \end{aligned}\right\} \tag{41}$$

Here suffix n represents functions evaluated at $(\bar{\omega}+\Delta\bar{\omega})$, while $n-1$ represents the known functions at $\bar{\omega}$. These equations are very similar to (26), containing only the additional terms involving $\Delta\bar{\omega}$. They have also been integrated using a fourth-order Runge–Kutta technique – it was necessary only to modify slightly the algorithm used earlier – starting with the low-frequency solution at $\bar{\omega} = 1$. However the increment $\Delta\bar{\omega}$ occurs in (39) and (40) in the denominator, and as $\bar{\omega}$ is increased, the coefficient $\bar{\omega}/\Delta\bar{\omega}$ increases, and the numerical solution becomes susceptible to rounding errors, particularly in the outer regions of the boundary layer. The inaccuracies increase, of course, with increasing $\bar{\omega}$, if $\Delta\bar{\omega}$ is kept constant. These errors can be contained by not using too small a value of $\Delta\bar{\omega}$, and by increasing it as $\bar{\omega}$ increases. Following some numerical experiments, computations were carried out, for $Q/U_\infty = 0.6$, varying the step size as the calculation progressed: $\Delta\bar{\omega} = 1$ from $\bar{\omega} = 1$ to $\bar{\omega} = 4$; $\Delta\bar{\omega} = 2$ from $\bar{\omega} = 4$ to $\bar{\omega} = 10$; and $\Delta\bar{\omega} = 5$ from $\bar{\omega} = 10$ to $\bar{\omega} = 30$. The results are shown in figures 7, 8 and 9.

Figure 7 shows that the sideslip velocity amplitude profiles using the intermediate frequency approximation agree closely with the low-frequency solution, for $1 < \bar{\omega} < 3$, and figure 8 shows that the relative phase ϕ_w, at the wall joins the low- and high-frequency solutions smoothly at $\bar{\omega} = 3$ and $\bar{\omega} = 10$ respectively. The

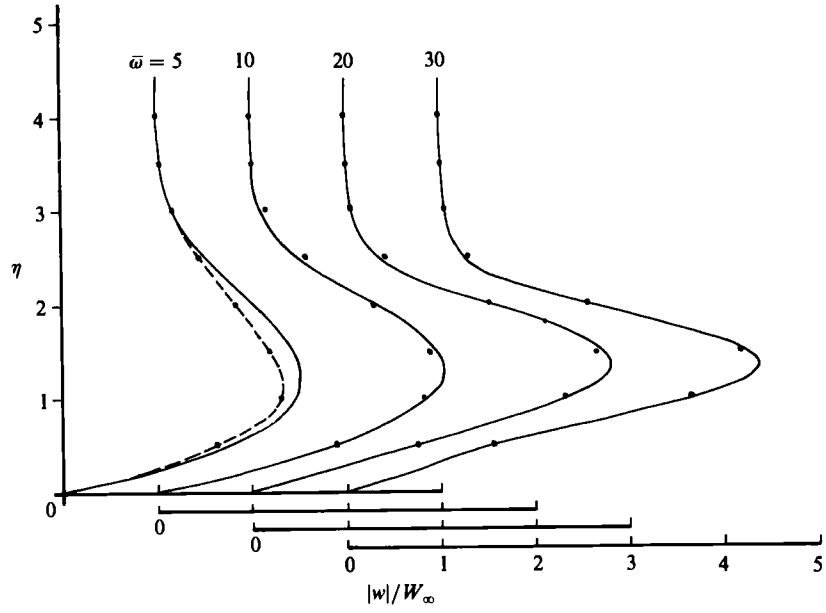

FIGURE 9. Normalized sideslip profiles, ——, high-frequency approximation, ●, intermediate-frequency solution.

intermediate- and high-frequency approximations to the amplitude profiles are compared in figure 9, and it can be seen that good agreement is achieved for $\bar{\omega} \geqslant 10$. One may note that the inclusion of the streamwise convection term $f'(\partial g/\partial \bar{\omega})$ in the solution has a negligible effect for $\bar{\omega} \geqslant 10$, justifying its neglect in the high-frequency approximation.

2.5. *Further discussion*

The fact that solutions for large $\bar{\omega}$ are virtually independent of streamwise convection is interesting, since it implies that the transverse flow far downstream at a fixed frequency ω is only weakly influenced by the upstream flow. The transverse component of the wall shear stress (skin friction) is given by

$$\tau_{yz} = \mu \frac{\partial w}{\partial y} \quad \text{at } y = 0,$$

so that using (10) we readily find that

$$\left[\frac{\tau_{yz}}{\frac{1}{2}\rho U_\infty^2}\right]_w (Re_x)^{\frac{1}{2}} = \frac{W_\infty}{U_\infty} \sqrt{2} \left[\frac{\partial g}{\partial \eta}\right]_w \exp i\omega\left(t - \frac{x}{Q}\right), \tag{42}$$

where $Re_x = U_\infty x/\nu$.

Likewise the longitudinal skin-friction component is given by the Blasius relation

$$\left[\frac{\tau_{xy}}{\frac{1}{2}\rho U_\infty^2}\right]_w (Re_x)^{\frac{1}{2}} = \sqrt{2} f''(0) = 0.6641. \tag{43}$$

Since the relative phase at the wall is calculated using the gradients $(\partial g/\partial \eta)_w$ the phase of the transverse wall friction is given by figure 8 for $Q/U_\infty = 0.6$. The magnitude of the transverse skin friction is proportional to $(\partial g/\partial \eta)_w$ and its amplitude is plotted in figure 10 as a function of $\bar{\omega}$, for $Q/U_\infty = 0.6$.

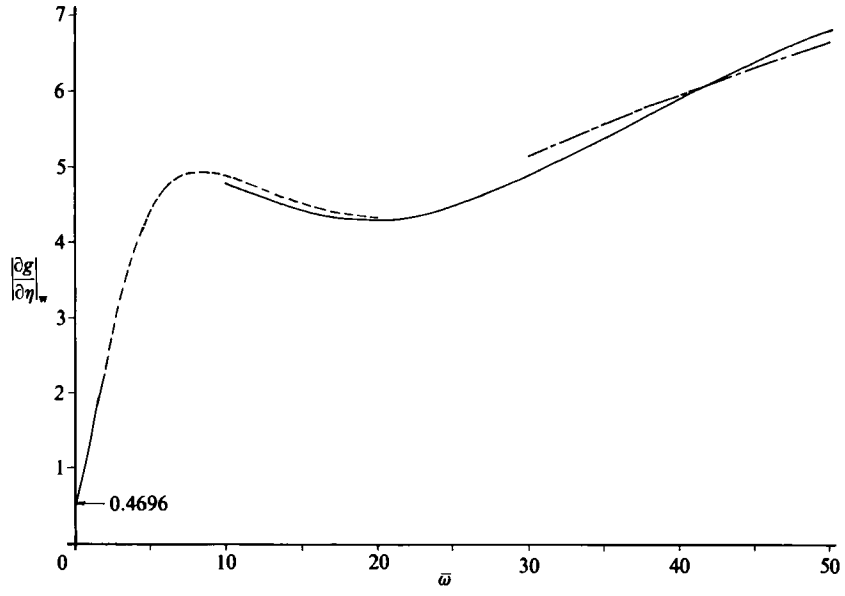

FIGURE 10. Amplitude of transverse skin-friction function for $Q/U_\infty = 0.6$; ----, intermediate-frequency solution; ——, equation (44).

We see that the amplitude of the transverse skin-friction coefficient multiplied by $(Re_x)^{\frac{1}{2}}$ initially increases rapidly with $\bar{\omega}$, before levelling off dipping a little, and then increasing again. For large values of $\bar{\omega}$, the increase appears to be nearly linear, but according to (20), at large $\bar{\omega}$.

$$\left|\frac{\partial g}{\partial \eta}\right|_w = \left|\left(1-\frac{U_\infty}{Q}\right)(2\bar{\omega})^{\frac{1}{2}}\right|, \tag{44}$$

so that

$$\left|\left(\frac{\tau_{yz}}{\frac{1}{2}\rho U_\infty^2}\right)_w (Re_x)^{\frac{1}{2}}\right| \to \frac{2W_\infty}{U_\infty}\left|\left(1-\frac{U_\infty}{Q}\right)\bar{\omega}^{\frac{1}{2}}\right|. \tag{45}$$

Equation (44) is also shown on figure 10 for $Q/U_\infty = 0.6$. Assuming the behaviour represented by (45) is correct, we see that for a fixed ω, the transverse component of the skin friction approaches a constant value while the longitudinal component decreases as $1/x^{\frac{1}{2}}$. Their ratio is

$$\left|\frac{\tau_{yz}}{\tau_{xy}}\right|_w = \frac{W_\infty}{U_\infty}\frac{1}{f''(0)}\left|\frac{\partial g}{\partial \eta}\right|_w = 2.13\frac{W_\infty}{U_\infty}\left|\frac{\partial g}{\partial \eta}\right|_w,$$

and since the analysis is applicable for arbitrary values of W_∞ it may reach significant values downstream even for moderate values of W_∞/U_∞.

Finally we may note that since the governing equation is linear in w, solutions for different frequencies may be added, and in principle at least, the response to an arbitrary sideslip function $w_\infty(t)$ computed.

3. Experiments

3.1. *Apparatus*

The experiments were conducted in the smallest of the QMC gust-tunnels, a blowdown wind-tunnel driven by a centrifugal fan powered by a 5.5 kW a.c. motor. Filtered air is passed to a settling chamber, equipped with wire screens and a honeycomb to

reduce turbulence, from which it enters a two-dimensional contraction nozzle of area ratio 6.25. The downstream end of the contraction is 200 mm in height and of width 800 mm. Contiguous with the upper and lower walls (roof and floor) at the nozzle exit is a pair of full-width flaps of chord 180 mm, hinged at their upstream end. Mechanically coupled together in-phase, they are driven sinusoidally by a $\frac{1}{2}$ h.p. d.c. motor, the speed of which is continuously variable to give oscillation frequencies between 2 Hz and 18 Hz. The test-section has sidewalls but no roof or floor. The static pressure in the 'semi-open' test region is thus essentially the ambient pressure in the laboratory. The mean wind-speed in the tunnel is controlled by a thyristor-controller giving a range from 3 m/s to 18.5 m/s.

The relevant performance characteristics in the unsteady mode are summarized in figure 11 (*a*, *b*) where the variations in the amplitude W_∞, of the sinusoidal upwash and in the wave velocity Q, are shown. It will be noted that the tests to be described were conducted in a region where Q is uniform and the amplitude W_∞ varies very little.

The flat plate model consisted of a stiffened, single sheet of aluminium, 2 mm in thickness, with one of its edges chamfered at 5° to provide a well-defined sharp leading edge. The plate was of chord 1000 mm and span 510 mm, so that mounted vertically in the centreplane of the test-section (that is, perpendicular to the flaps), the chordwise edges were well outside the flow. It was provided with pressure tappings and a trailing-edge flap so that it could be set with zero pressure gradient and with the stagnation point on the plane, unchamfered surface just aft of the leading edge, which was positioned 165 mm downstream of the trailing-edges of the nozzle flaps, so as to be in the region in which Q/U_∞ is fairly uniform.

The mounting ensured that with the nozzle flaps oscillating, no signs of vibration of the plate were apparent.

The frequency of oscillation of the flaps was measured by means of a slotted disk mounted on the final drive shaft to the flaps. The edge of this disk passed between the infra-red source and detector of an optical switch enabling a resolution of 0.01 Hz to be achieved.

A flattened pitot tube and a constant-temperature, hot-wire anemometer probe together with a linearizer circuit and a digital voltmeter were used for checking the steady laminar boundary-layer velocity profile and also for calibrating the probe-positioning device as will be explained in §3.2.

A single hot-wire probe and linearizer were also used to investigate the oscillatory boundary layer, the wire being orientated parallel to the surface of the plate but at 45° to its leading edge. Such an anemometer probe responds to both the streamwise, u-component and the transverse, w-component of velocity. However the u-component is steady while the w-component is purely oscillatory, so that the latter is easily extracted using a d.c. blocking filter.

All the probes were positioned using a manually-operated screw (Unislide) having a resolution of 0.01 mm in the direction perpendicular to the plate.

The relative phase $\phi(\eta)-\phi(\infty)$ was measured by a specially-developed, digital phase meter, since no instrument was available with the required resolution at low frequencies. Essentially this phase meter measures the average time between the zero-crossings of the a.c. components of the measuring and reference signals and compares this with the period of the oscillations. The instrument, which is more fully described by Ishaq (1984), has a resolution better than 1° at all the frequencies of interest here. It was also used to measure the wave speed Q, using two hot-wire anemometers a known distance apart.

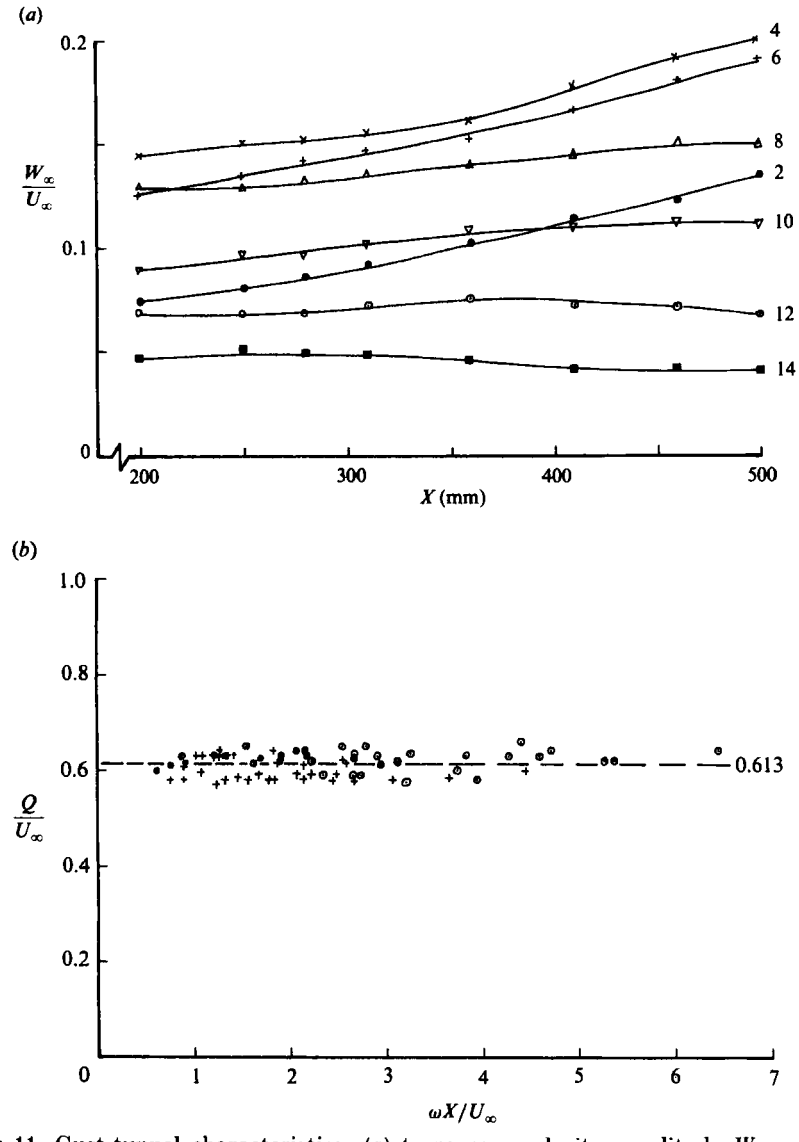

FIGURE 11. Gust-tunnel characteristics: (*a*) transverse velocity amplitude W_∞, *vs.* distance X, downstream of the nozzle exit and frequency/Hz (indicated on figure) for $U_\infty = 5.19$ m/s; (*b*) wave velocity ratio Q/U_∞ *vs.* $\omega X/U_\infty$; ⊙, $U_\infty = 5.19$ m/s; +, $U_\infty = 13.3$ m/s.

3.2. *Preliminary experiments and calibrations*

With the trailing-edge flap set at about 7°, the pressure gradient in steady flow was less than 1 mmH_2O/m, and it was maintained at this angle for all the subsequent experiments. Using the flattened Pitot tube several velocity profiles $u(y)$, were measured to gauge the extent of the laminar boundary-layer region. The Pitot was then replaced by a single hot-wire anemometer for more detailed measurements.

One of the difficulties associated with using a hot-wire probe for boundary-layer studies is measuring accurately its distance y, from the surface. Because of its fragility it cannot be allowed to touch the plate, so its 'initial' position is somewhat uncertain even though incremental distances can be set very accurately. This problem was

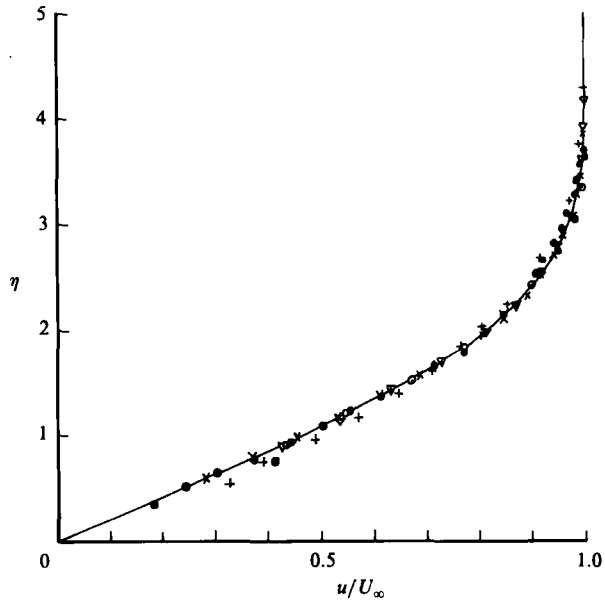

FIGURE 12. Measured steady velocity profiles at $(U_\infty x/\nu) \times 10^{-5} = \nabla$, 0.35; ⊙, 0.71; ×, 0.77; +, 1.20; ●, 1.32. ——, Blasius profile.

overcome in the following way. The steady velocity profile data, plotted using Blasius coordinates were found to follow closely the Blasius profile, see figure 12. All subsequent steady profiles were assumed to be similar in the laminar boundary-layer region. Before making unsteady measurements at any station, a steady profile was measured and used to calibrate the 'initial' probe position; other positions were given by incremental settings on the micrometer screw. The probe and linearizer were frequently checked for zero-offset and linearity of voltage output with windspeed, so that velocity ratios could be obtained easily.

With the test-section semi-open, the upper and lower boundaries were free-mixing shear layers. The spread of these turbulent mixing regions restricted the spanwise extent of the laminar boundary layer growing on the plate. With the nozzle flaps stationary at both their extreme positions, the encroachment of the mixing regions into the core flow was measured. Steady boundary-layer profiles were also measured 50 mm off the centreline at several distances from the leading edge and the hot-wire output was observed on a CRO for signs of turbulence over a wide region near the surface of the plate. In this way one could ensure that the experiments in the periodically-driven boundary layer were conducted in a laminar region.

3.3. *Experiments in the unsteady boundary layer*

All the unsteady measurements in the boundary layer were conducted on the centreplane. Most of them were made at a single station, 110 mm from the leading edge at a mean windspeed of 5.1 m/s, thus ensuring a reasonably thick boundary layer, about 2.5 mm, in which to work. At each distance y, from the surface the flap oscillation frequency was varied in the range 4–18 Hz and the phase measured. Each result is the mean of ten successive readings, the number of cycles over which each reading was averaged by the phase meter being 80. For most of the measurements the reference oscillation was provided by a displacement transducer following the

motion of the flaps. Some measurements were repeated with a second hot-wire probe, outside the boundary layer and somewhat upstream, providing the reference signal. Additional measurements were made further from the leading edge and at appropriate mean wind speeds U_∞, but it was only possible to cover the range of reduced frequency $\bar{\omega} = \omega x/U_\infty$, up to 2.0. Measurements of the amplitude profiles $w(y)$, were made under similar conditions during separate traverses.

4. Analysis and discussion of results

From the steady laminar boundary-layer velocity profiles shown in figure 12 one may conclude that the boundary layer is laminar for Reynolds numbers $U_\infty x/\nu$, up to at least 10^5 and was laminar for the unsteady measurements which were made at Reynolds numbers well below this. Figure 12 also justifies the use of the Blasius profile for calibrating the probe.

The regions of turbulence nearest to the measuring stations, arise from the mixing in the free shear layer bounding the upper and lower edges of the test region, but they are believed to be sufficiently far away as not to affect the unsteady laminar boundary-layer results. This belief is justified by the steady results shown in figure 12 and also by the unsteady results themselves.

A large body of data for the laminar boundary layer on the plate with the external flow in periodic sideslip was collected essentially as curves of relative amplitude and phase along lines of constant η (or y) and varying $\bar{\omega}$, for $\bar{\omega} \leqslant 1$. The phase reference for these measurements was taken from the flap motion. For comparison with the theoretical predictions these data were cross-plotted to give the relative phase $\phi(\eta) - \phi(\infty)$, and amplitude ratio $w(\eta)/W_\infty$, profiles for constant $\bar{\omega}$. The values of $\phi(\infty)$ and W_∞ were taken as equivalent to those measured at $\eta \approx 4$ since no further changes were detected for greater values. Data for $\bar{\omega} = 1.5$ and 2.0 were obtained by appropriately setting the values of ω, x and U_∞ to achieve these values. The results are summarized in figures 13 and 14 which also show the computed profiles for comparison.

Although the phase measurements were effectively the result of averaging over 800 cycles of the external flow oscillation, the data, open symbols on figure 13, for $\bar{\omega} = 0.8$ and $\bar{\omega} = 1.0$ showed unexpectedly large scatter. It was suspected that this arose from the use of the flap motion to provide a phase reference, the relative phases being the differences of comparatively large values. A second hot-wire probe was therefore used, outside the boundary layer and 103 mm upstream of the measuring probe, to provide the phase reference for a repeated set of measurements at $\bar{\omega} = 0.8$ and $\bar{\omega} = 1.0$. These data are shown as filled symbols on figure 13. The scatter is somewhat reduced, but there was a further advantage because with the measuring probe also outside the boundary layer, the measured phase shift represents the wave-speed ratio Q/U_∞. The particular values measured in these cases were $Q/U_\infty = 0.544$ at $\bar{\omega} = 0.8$ and $Q/U_\infty = 0.568$ at $\bar{\omega} = 1.0$ and the corresponding theoretical curves are also shown in figure 13. The sensitivity of the phase to Q/U_∞ diminishes with increasing $\bar{\omega}$ and no corresponding calculations and measurements have been conducted for $\bar{\omega} > 1.0$.

The results confirm not only that there is a transverse (sideslip) velocity phase lag within the boundary layer for $Q/U_\infty \approx 0.6$, but also shows that the theory predicts the values quite well.

Similarly good agreement is demonstrated in figure 14 between the measured and computed transverse velocity amplitude ratio profiles, which are much less sensitive to Q/U_∞. As predicted there is an amplification factor greater than one in part of

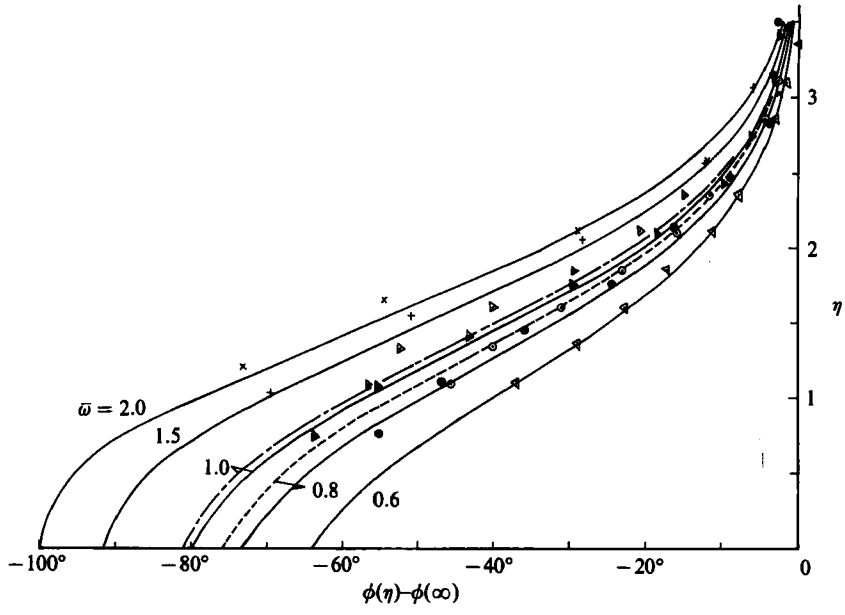

FIGURE 13. Relative phase profiles: Experiment: ◁, $\bar{\omega} = 0.6$; ⊙●, $\bar{\omega} = 0.8$; ▷ ▶, $\bar{\omega} = 1.0$; +, $\bar{\omega} = 1.5$; ×, $\bar{\omega} = 2.0$. Theory: ——, $Q/U_\infty = 0.6$; —·—, $Q/U_\infty = 0.568$; – – –, $Q/U_\infty = 0.544$.

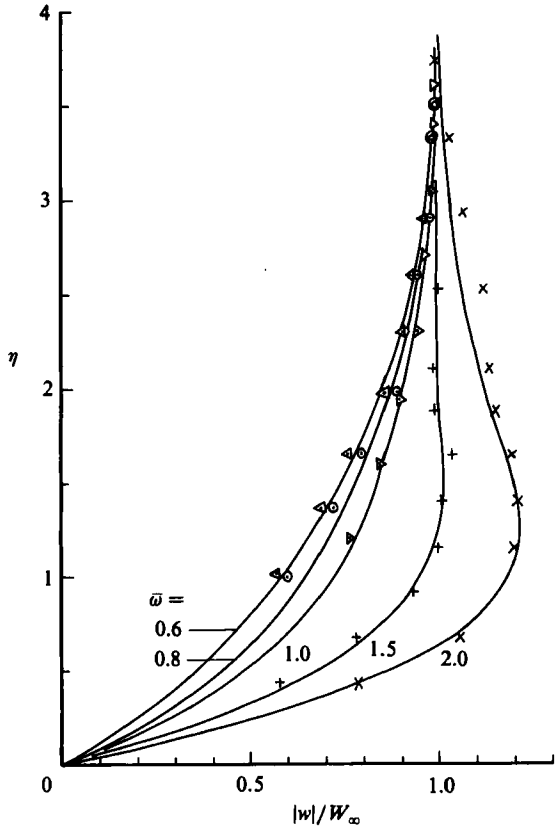

FIGURE 14. Normalized amplitude profiles. (See figure 13 for key to symbols.) Theoretical curves are for $Q/U_\infty = 0.6$.

the boundary layer for reduced frequencies $\bar{\omega}$ greater than about 1.5 at $Q/U_\infty \approx 0.6$, and this amplification increases with $\bar{\omega}$. Since $\bar{\omega} = \omega x/U_\infty$ may be regarded as the streamwise coordinate at constant frequency ω, the maximum amplitude of the oscillation within the boundary layer increases with distance downstream as predicted, at least up to $\bar{\omega} = 2.0$.

One may also conclude that the small variation of the amplitude W_∞, of the imposed transverse velocity oscillation with distance x downstream (see figure 11*a*), has very little effect on the results.

5. Conclusions

The analysis has shown that with a finite wave velocity, the longitudinal flow is independent of the oscillatory transverse (sideslip) flow.

This transverse flow is governed by a linear partial differential equation in two independent variables which may be further reduced to an ordinary differential equation for the two extremes of high- and low-frequency parameter $\bar{\omega} = \omega x/U_\infty$. For $\bar{\omega}$ small, a series-expansion solution appears to be valid up to $\bar{\omega} \approx 2$; the large $\bar{\omega}$ approximation, obtained by neglecting the streamwise convection term, is valid down to $\bar{\omega} \approx 10$. A differential-difference equation has been used for the range $1 < \bar{\omega} < 10$, and this joins the other solutions smoothly.

For $Q/U_\infty < 1$ and $\bar{\omega} = 10$ there are large phase lags within the boundary layer compared with the external driving flow; for large values of the wave-speed ratio, there are phase leads within most of the viscous layer the changeover from lag to lead occurring very near, but not at $Q/U_\infty = 1$.

At low values of $\bar{\omega}$ the changeover from lag to lead is complicated, but at the wall occurs at $Q/U_\infty \approx 1.23$.

The sideslip velocity amplitude profiles are also critically dependent upon the wave-speed ratio, large 'overshoots' appearing for low values of Q/U_∞; at $Q/U_\infty = 0.6$, the peak amplitude within the viscous layer is more than three times that of the driving oscillation.

As $\bar{\omega}$ becomes very large, the transverse oscillatory boundary layer becomes very thin; it is then a 'Stokes shear layer' and is virtually uncoupled from the longitudinal flow. Also for large $\bar{\omega}$ the downstream transverse flow is only weakly dependent on the upstream conditions, and the amplitude of the transverse skin friction can reach values comparable with the local longitudinal skin friction.

Measurements have been made, at values of the frequency parameter $\bar{\omega} = \omega x/U_\infty$ up to 2.0. The relative phase and amplitude profiles are in very good agreement with those predicted. In particular the measurements confirm that there are phase lags within the boundary layer for travelling-wave velocities $Q \approx 0.6U_\infty$, in contrast to the phase leads predicted for the standing-wave case ($Q \to \infty$) and also that for $\bar{\omega} > 1.5$ approximately, there are sideslip velocity amplification factors greater than one for $Q \approx 0.6U_\infty$.

The authors would like to express their gratitude to Dr H. P. Horton for several very useful discussions and to Dr T. J. Pedley and the referees for their contributions to the high frequency analysis.

One of us (M.S.I.) must thank the Africa Educational Trust and the United Arab Emirates for financial support.

REFERENCES

ABRAMOWITZ, M. & STEGUN, I. A. 1965 *Handbook of Mathematical Functions*. Dover.

ACKERBERG, R. C. & PHILLIPS, J. H. 1972 The unsteady laminar boundary layer on a semi-infinite flap plate due to small fluctuations in the magnitude of the free stream velocity. *J. Fluid Mech.* **51**, 137–157.

BERNSTEIN, L. 1984 On the laminar boundary layer on a flat plate in periodic sideslip. Queen Mary College EP-1062.

FARN, C. L. S. & ARPACI, V. S. 1965 On the numerical solution of unsteady laminar boundary layers. *AIAA J.* **4**, 730–732.

GHOSH, A. 1961 Contribution à l'étude de la couche limite laminaire instationnaire. *Pub. Sci. et Tech. du Min. del' Air*, no. 381.

HILL, P. G. & STENNING, A. H. 1960 Laminar boundary layers in oscillatory flow. *Trans. ASME* D: *J. Basic Engng* **82**, 593–608.

ISHAQ, M. S. 1984 An investigation of some flows in an oscillatory flow wind tunnel. M.Phil. thesis, University of London.

LAM, C. Y. 1983 Unsteady laminar and turbulent boundary layer computations using a differential-difference method. Ph.D. thesis, University of London.

LIGHTHILL, M. J. 1954 The response of laminar skin-friction and heat transfer to fluctuations in the stream velocity. *Proc. R. Soc. Lond.* A**224**, 1–23.

LIN, C. C. 1957 Motion in the boundary layer with a rapidly oscillating external flow. *Proc. 9th Intl Cong. Appl. Mech., Brussels*, pp. 155–167.

MOORE, F. K. 1957 Aerodynamic effects of boundary layer unsteadiness. *VIth Anglo-American Aeronautical Conference, Folkestone*. R.Ae.S.

NICKERSON, R. J. 1957 The effect of free stream oscillations on the laminar boundary layer on a flat plate. Sc.D. thesis, M.I.T.

PATEL, M. H. 1975 On laminar boundary layers in oscillatory flow. *Proc. R. Soc. Lond.* A**347**, 99–123.

PATEL, M. H. 1977 On turbulent boundary layers in oscillatory flow. *Proc. R. Soc. Lond.* A**353**, 121–144.

PATEL, M. H. & HANCOCK, G. J. 1976 A gust-tunnel facility. *Aero. Res. Counc.* R & M 3802. HMSO.

PEDLEY, T. J. 1972 Two-dimensional boundary layers in a free stream which oscillates without reversing. *J. Fluid Mech.* **55**, 359–383.

ROTT, N. & ROSENZWEIG, M. L. 1960 On the response of the laminar boundary layer to small fluctuations of the free-stream velocity. *J. Aerospace Sci.* **27**, 741–747.

SCHLICHTING, H. 1979 *Boundary Layer Theory*. McGraw-Hill.

STEWARTSON, K. 1960 The theory of unsteady laminar boundary layers. *Adv. Appl. Mech.* **6**, 1–37.

STOKES, G. G. 1851 On the effect of the internal friction of fluids on the motion of pendulums. *Trans. Camb. Phil. Soc.* **9**, 8–106.

TEIPEL, I. 1970 Calculation of unsteady laminar boundary layers by an integral method. *Z. Flugwiss.* **18**, 58–65.

TELIONIS, D. 1981 *Unsteady Viscous Flows*. Springer.

WUEST, W. 1952 Grenzschichten an zylindrischen Korpen mit nichtstationarer Querbewegung. *Z. Angew. Math. Mech.* **32**, 172–178.